Title
A Hypothalamic Switch for REM and Non-REM Sleep

Journal
Neuron, 97(5)

ISSN
0896-6273

Authors
Chen, Kai-Siang
Xu, Min
Zhang, Zhe
et al.

Publication Date
2018-03-01

DOI
10.1016/j.neuron.2018.02.005

Peer reviewed

Article

Neuron

A Hypothalamic Switch for REM and Non-REM Sleep

Highlights

- DMH galaninergic neurons consist of two distinct populations—REM-on and REM-off
- Separate DMH galaninergic neurons project to POA and RPA
- The POA-projecting neurons are REM-off, and their activity suppresses REM sleep
- The RPA-projecting neurons are REM-on, and their activity promotes REM sleep

Authors

Kai-Siang Chen, Min Xu, Zhe Zhang, Wei-Cheng Chang, Thomas Gaj, David V. Schaffer, Yang Dan

Correspondence

ydan@berkeley.edu

In Brief

Using microendoscopic calcium imaging and bidirectional optogenetic manipulation, Chen et al. showed that galaninergic neurons in the dorsomedial hypothalamus consist of two subpopulations with distinct axon projections and opposing roles in regulating the switch between REM and non-REM sleep.

Chen et al., 2018, Neuron *97*, 1168–1176
March 7, 2018
https://doi.org/10.1016/j.neuron.2018.02.005

CellPress

CellPress

Neuron
Article

A Hypothalamic Switch for REM and Non-REM Sleep

Kai-Siang Chen,[1,2,4] Min Xu,[1,2,4,5] Zhe Zhang,[1,2] Wei-Cheng Chang,[1,2] Thomas Gaj,[1,3] David V. Schaffer,[1,3] and Yang Dan[1,2,6,*]

[1]Division of Neurobiology, Department of Molecular and Cell Biology, Helen Wills Neuroscience Institute, University of California, Berkeley, CA 94720, USA

[2]Howard Hughes Medical Institute, University of California, Berkeley, CA 94720, USA

[3]Department of Chemical and Biomolecular Engineering, University of California, University of California, Berkeley, CA 94720, USA

[4]These authors contributed equally

[5]Present address: Institute of Neuroscience, State Key Laboratory of Neuroscience, Key Laboratory of Primate Neurobiology, CAS Center for Excellence in Brain Science and Intelligence Technology, Shanghai Institutes for Biological Sciences, Chinese Academy of Sciences, Shanghai 200031, China

[6]Lead Contact

*Correspondence: ydan@berkeley.edu

https://doi.org/10.1016/j.neuron.2018.02.005

SUMMARY

Rapid eye movement (REM) and non-REM (NREM) sleep are controlled by specific neuronal circuits. Here we show that galanin-expressing GABAergic neurons in the dorsomedial hypothalamus (DMH) comprise separate subpopulations with opposing effects on REM versus NREM sleep. Microendoscopic calcium imaging revealed diverse sleep-wake activity of DMH GABAergic neurons, but the galanin-expressing subset falls into two distinct groups, either selectively activated (REM-on) or suppressed (REM-off) during REM sleep. Retrogradely labeled, preoptic area (POA)-projecting galaninergic neurons are REM-off, whereas the raphe pallidus (RPA)-projecting neurons are primarily REM-on. Bidirectional optogenetic manipulations showed that the POA-projecting neurons promote NREM sleep and suppress REM sleep, while the RPA-projecting neurons have the opposite effects. Thus, REM/NREM switch is regulated antagonistically by DMH galaninergic neurons with intermingled cell bodies but distinct axon projections.

INTRODUCTION

Rapid eye movement (REM) and non-REM (NREM) sleep are distinct brain states associated with different mental experience and functional roles (Brown et al., 2012). During NREM sleep, the electroencephalogram (EEG) is dominated by large-amplitude slow-wave activity, but during REM sleep the EEG is desynchronized (Aserinsky and Kleitman, 1953; Dement, 1958; Jouvet, 1962). The switch between REM and NREM sleep occurs multiple times each day, but the neural circuit controlling the switch remains poorly understood.

REM and NREM sleep are regulated by multiple groups of neurons in the brainstem and hypothalamus (Brown et al., 2012; Jouvet, 1962; Saper et al., 2010; Scammell et al., 2017; Weber and Dan, 2016). In the brainstem, some neurons powerfully promote NREM to REM transitions, while others sustain NREM sleep and suppress REM sleep (Anaclet et al., 2014; Boissard et al., 2003; Clément et al., 2011; Hayashi et al., 2015; Hobson et al., 1975; Lu et al., 2006; Sapin et al., 2009; Sastre et al., 1996; Van Dort et al., 2015; Weber et al., 2015). In the lateral hypothalamus, melanin-concentrating hormone (MCH)-expressing neurons are most active during REM sleep (Hassani et al., 2009). Their brief optogenetic activation strongly promotes REM sleep, while their chronic activity is found to be important for NREM sleep (Blanco-Centurion et al., 2016; Ferreira et al., 2017; Jego et al., 2013; Konadhode et al., 2013; Tsunematsu et al., 2014). The dorsomedial hypothalamus (DMH) also plays a key role in sleep regulation, as its lesion decreased both NREM and REM sleep during the subjective day but have the opposite effects during the subjective night (Aston-Jones et al., 2001; Chou et al., 2003). However, the underlying circuit mechanism is not well understood. Neurons in the DMH exhibit diverse brain-state-dependent firing patterns (Findlay and Hayward, 1969), which is partly due to the existence of multiple cell types. A recent study using single-cell RNA sequencing showed that, as a molecular marker, galanin labels a subtype of GABAergic neurons in the hypothalamus (Romanov et al., 2017). This neuropeptide is strongly implicated in sleep regulation (Sherin et al., 1998; Steiger and Holsboer, 1997), and it is densely expressed in the DMH.

In this study, we examined the role of galanin-expressing DMH neurons in sleep regulation using microendoscopic calcium imaging, virus-assisted circuit tracing, and bidirectional optogenetic manipulations. We found that while DMH GABAergic neurons exhibit diverse brain-state-dependent activity, the galanin-expressing subpopulation consists of two distinct groups with opposing effects on REM versus NREM sleep. These two neuronal groups can be separated on the basis of their axonal projections, but their cell bodies are intermingled in the DMH. The physical proximity between these functionally antagonistic populations could facilitate their reciprocal inhibitory interactions to induce the rapid switch between REM and NREM sleep.

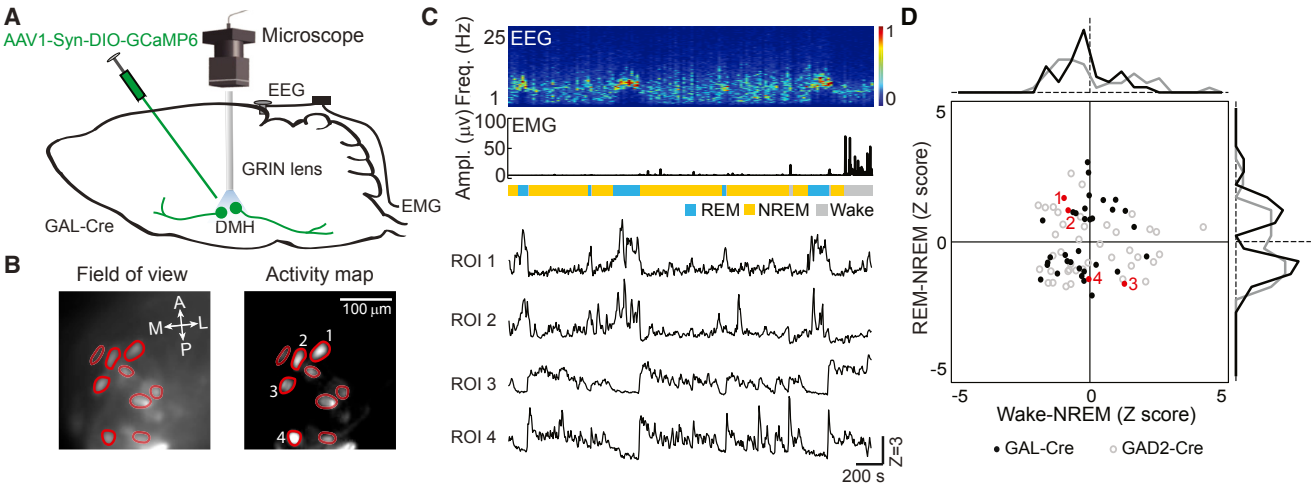

Figure 1. DMH Galaninergic Neurons Consist of Distinct REM-On and REM-Off Subpopulations

(A) Schematic of microendoscopic calcium imaging in the DMH.

(B) Field of view (left) and activity map (right) of an example imaging session in a GAL-Cre mouse. M, medial; L, lateral; A, anterior; P, posterior. Regions of interest (ROIs) are outlined in red. Numbers indicate ROIs whose calcium traces are plotted in (C).

(C) EEG power spectrogram, EMG trace, brain states (color coded), and calcium traces (*Z* scored) recorded in the imaging session.

(D) REM-NREM activity difference versus wake-NREM activity difference. Each symbol represents one neuron. Red, galaninergic neurons shown in (C). Black, galaninergic neurons from GAL-Cre mice (n = 36 neurons from 4 mice). Gray, GABAergic neurons from GAD2-Cre mice (n = 40 neurons from 3 mice). Traces on the top and right, distributions of wake-NREM (top) and REM-NREM (right) activity difference for galaninergic (black) and GABAergic (gray) neurons.

See also Figures S1 and S2.

RESULTS

Microendoscopic Calcium Imaging of DMH Neurons

To measure the activity of DMH galaninergic neurons across brain states, we used a galanin (GAL)-Cre mouse line (Gerfen et al., 2013), in which the specificity of GAL-Cre expression in the DMH has been validated previously by *in situ* hybridization (2011 Allen Institute for Cell Science, Allen Mouse Brain Connectivity Atlas, available from http://connectivity.brain-map.org/transgenic/experiment/100138525). A Cre-inducible adeno-associated virus (AAV) expressing the calcium indicator GCaMP6f (Chen et al., 2013) was injected into the DMH (Figure S1A), and imaging was performed through a gradient refractive index (GRIN) lens coupled to a miniaturized integrated fluorescence microscope in freely moving mice (Cox et al., 2016; Ghosh et al., 2011). During each imaging session, brain states were classified based on EEG and electromyogram (EMG) recordings (Figures 1A and 1B). Calcium activity of the galaninergic neurons varied strongly across brain states (Figure 1C). In particular, for each of the 36 imaged neurons, the activity was significantly different between REM and NREM sleep ($p < 0.05$, Wilcoxon rank-sum test). Some neurons were selectively activated during REM sleep ("REM-on" neurons), while others were selectively suppressed ("REM-off" neurons). These neurons were often observed in the same field of view (Figures 1B and 1C), and they appeared to be spatially intermingled (Figure S1B).

To quantify the relative activity of each neuron in different brain states, we plotted its REM-NREM modulation index ($Z_{REM} - Z_{NREM}$, where Z is Z-scored calcium activity averaged within each brain state) versus the wake-NREM modulation index ($Z_{wake} - Z_{NREM}$). The galaninergic neurons fell into two distinct clusters (Figure 1D, black dots). The REM-NREM modulation index exhibited a clear bimodal distribution ($p = 0.003$, Hartigan's dip test), with the two peaks corresponding to the REM-on and REM-off neurons. However, the wake-NREM modulation index showed a unimodal distribution centered around 0 ($p = 0.98$, Hartigan's dip test), indicating that the overall activity was similar during wakefulness and NREM sleep.

Interestingly, when we imaged the sleep-wake activity of DMH GABAergic neurons in GAD2-Cre mice, we found a much higher degree of functional heterogeneity, with different neurons preferentially active during wake, REM, or NREM states (Figure S2). Both the REM-NREM and wake-NREM modulation indices showed unimodal distributions ($p = 0.60$, Hartigan's dip test), and the GABAergic neurons were scattered in all quadrants with no apparent clustering (Figure 1D, gray dots). This suggests that, as a subpopulation of DMH GABAergic neurons, the galaninergic neurons are especially involved in regulating REM and NREM sleep.

Axon Projections of DMH Galaninergic Neurons

Given the similar transmitter phenotypes of REM-on and REM-off DMH neurons (both are GABAergic and galaninergic), we wondered whether they can be distinguished based on their projection targets. Anterograde tracing of DMH galaninergic axons using Cre-inducible AAV expressing enhanced yellow fluorescent protein (eYFP) revealed projections to multiple brain regions, including the preoptic area (POA), lateral hypothalamus (LHA), dorsomedial region of the thalamus, periaqueductal gray (PAG), dorsolateral pons, and raphe pallidus (RPA) (Figures S3A and S3B). Such broad projections are consistent with previous findings in the rat (Aston-Jones et al., 2001; Chou et al., 2003).

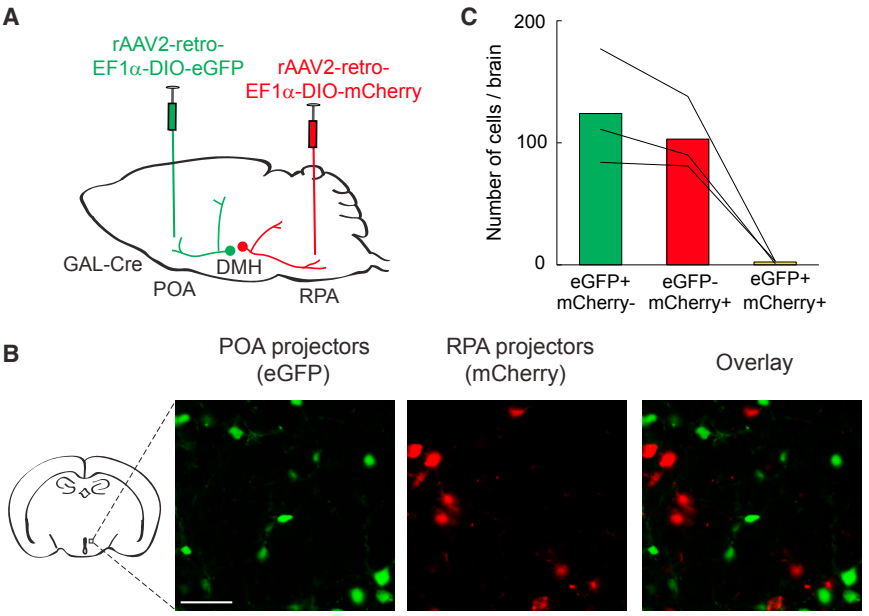

Figure 2. POA-Projecting and RPA-Projecting DMH Galaninergic Neurons Are Distinct Subpopulations

(A) Schematic of viral injection for simultaneous retrograde tracing from POA and RPA.

(B) Fluorescence images of DMH showing neurons expressing eGFP and mCherry. Scale bar, 50 μm.

(C) Number of neurons expressing each marker alone or both. Each line represents data from one mouse (n = 3 mice).

See also Figure S3.

To determine whether these divergent projections originate from different subsets of DMH neurons or reflect collateral projections from the same population, we selectively labeled the neurons projecting to each area. Since our anterograde tracing experiment showed the most extensive galaninergic projection to the POA, and previous studies indicated the importance of the DMH-POA pathway in sleep regulation (Chou et al., 2003), we first targeted the POA-projecting DMH neurons. An AAV vector expressing avian-specific retroviral receptor (TVA) fused with mCherry (AAV2-CAG-DIO-TVA-mCherry) was injected into the DMH of GAL-Cre mice, and a glycoprotein (G)-deleted, EnvA-pseudotyped rabies virus (RV) expressing enhanced green fluorescent protein (RV-ΔG-eGFP+EnvA) was injected into the POA to infect the TVA-expressing galaninergic neurons that project to the POA (Miyamichi et al., 2011; Zhang et al., 2016) (Figure S3C). Analysis of eGFP-labeled axons showed that, in addition to the POA, these DMH neurons also project to the LHA and thalamus (Figures S3D and S3G). However, in the RPA region we found no labeled axon. Conversely, when we performed the complementary experiments to label the RPA-projecting DMH neurons by injecting RV-ΔG-eGFP+EnvA into the RPA (Figure S3E), we found few eGFP-labeled axons in the POA (Figures S3F and S3H), suggesting that the POA and RPA projections originate from different neurons.

To test directly the relationship between the DMH neurons projecting to the POA and RPA, we performed simultaneous retrograde tracing from the two target areas. After injecting Cre-inducible rAAV2-retro (a designer AAV variant with high retrograde efficiency) (Tervo et al., 2016) expressing eGFP and mCherry into the POA and RPA, respectively (Figure 2A), we found strong expression of both eGFP and mCherry in the DMH but very little overlap between them (Figures 2B and 2C). This indicates that the POA- and RPA-projecting DMH galaninergic neurons form largely distinct subpopulations.

Activity of POA- and RPA-Projecting Neurons

We next measured the sleep-wake activity of the POA- or RPA-projecting subpopulation using calcium imaging. Cre-inducible rAAV2-retro expressing GCaMP6s was injected into the POA or RPA of GAL-Cre mice, and a GRIN lens was implanted into the DMH (Figures 3A, 3B, 3E, and 3F). Both subpopulations of DMH galaninergic neurons showed brain-state-dependent calcium activity. The POA-projecting neurons were selectively suppressed during REM sleep (Figures 3C and 3D), with all 28 cells showing lower activity during REM than NREM sleep (mean $\Delta Z = 1.4$, 95% confidence intervals [CIs] [1.2, 1.6]; $p < 0.001$, Wilcoxon rank-sum test), and 26/28 cells showing lower activity during REM sleep than wakefulness (mean $\Delta Z = 0.8$, 95% CIs [0.5, 1.0]; $p < 0.05$, Wilcoxon rank-sum test). In contrast, most of the RPA-projecting neurons were selectively activated during REM sleep (Figures 3G and 3H), with 52/55 showing higher activity during REM sleep than both NREM sleep (mean $\Delta Z = 2.9$, 95% CIs [2.5, 3.2]) and wakefulness (mean $\Delta Z = 2.6$, 95% CIs [2.2, 3.0]). For both the POA- and RPA-projecting subpopulations, the wake-NREM modulation index showed unimodal distributions around 0. Thus, the two galaninergic subpopulations defined by their projection targets largely segregate into the REM-on and REM-off functional categories.

POA-Projecting Neurons Suppress REM and Promote NREM Sleep

To test whether each subpopulation of DMH neurons play any causal role in sleep regulation, we manipulated their activity optogenetically. To express channelrhodopsin 2 (ChR2) in the POA-projecting neurons, we injected Cre-inducible rAAV2-retro-ChR2-eYFP into the POA of GAL-Cre mice and implanted an optic fiber into the DMH (Figures 4A and S4A). Laser stimulation (5 or 20 Hz, 2 min/trial, randomly applied every 5–30 min) caused a significant decrease in REM sleep (mean −7.6%, 95% CIs [−5.2%, −10.2%]; $p < 0.001$, bootstrap) and a complementary increase in NREM sleep (mean 11.7%, 95% CIs [8.5%, 14.8%], $p < 0.001$), with no significant change in wakefulness ($p > 0.18$; Figures 4B, 4C, and S5A). To distinguish whether the laser-induced suppression of REM sleep was due to a decrease in its initiation or maintenance, we analyzed the transition probability between each pair of brain states (Figure S4B). Laser activation

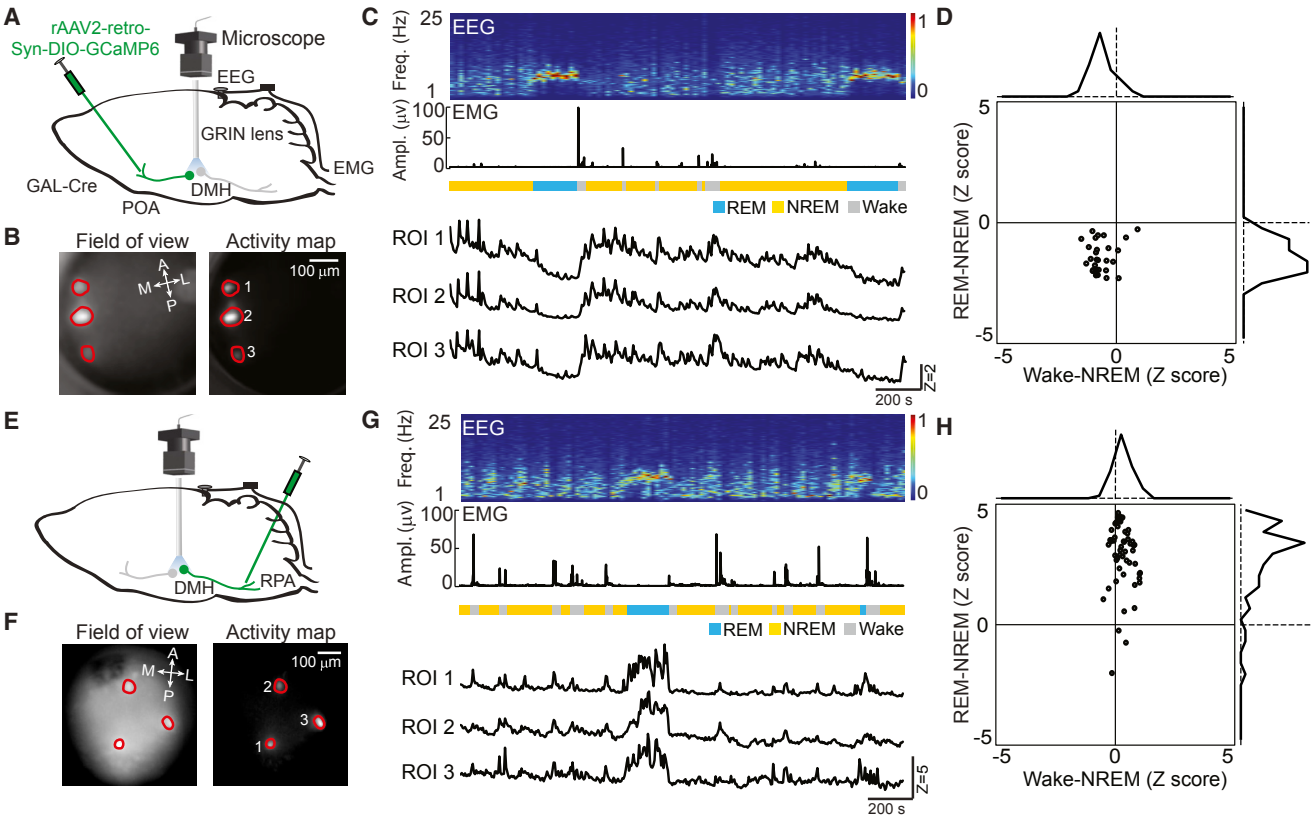

Figure 3. POA- and RPA-Projecting DMH Galaninergic Neurons Are REM-Off and REM-On, Respectively

(A) Schematic of calcium imaging of POA-projecting DMH galaninergic neurons.

(B) Field of view (left) and activity map (right) of an example imaging session. ROIs are outlined in red. Numbers indicate ROIs whose calcium traces are plotted in (C).

(C) EEG power spectrogram, EMG trace, brain states (color coded), and calcium traces (*Z* scored) recorded in the imaging session.

(D) REM-NREM activity difference versus wake-NREM activity difference. Traces on the top and right: distributions of wake-NREM and REM-NREM activity differences for POA-projecting DMH galaninergic neurons (n = 28 cells from 3 mice).

(E–H) Similar to (A)–(D), for RPA-projecting neurons (n = 55 cells from 3 mice).

of the POA-projecting neurons caused marked ($p < 0.05$, bootstrap) decreases in NREM→REM (mean –0.6%, 95% CIs [−0.4%, –0.7%]) and REM→REM transitions (mean –3.8%, 95% CIs [−3.6%, –4.1%]), indicating a suppression of both the initiation and maintenance of REM sleep (Figure 4D). To further quantify the reduction of REM sleep initiation, we calculated the percentage of times a NREM→REM transition occurred during the 2-min laser stimulation period (number of transitions during laser divided by the total number of transitions recorded). It was found to be much lower than the percentage during the 2-min window immediately before the laser stimulation (1.2% versus 8.2%).

Since the rAAV2-retro-DIO-ChR2-eYFP injected into the POA can also infect POA-projecting neurons outside of the DMH, in principle the effect of laser stimulation in the DMH could be mediated by the axons of these non-DMH neurons that pass through the DMH. We thus tested the effect of activating DMH neuron axons in the POA. Following the injection of AAV2-EF1α-DIO-ChR2-eYFP into the DMH of GAL-Cre mice, which labels only the DMH neurons, laser stimulation of their axons in the POA also suppressed REM sleep (mean –4.9%, 95% CIs [−3.1%, –6.8%], $p < 0.001$) and promoted NREM sleep (mean 6.9%, 95% CIs [4.3%, 9.5%], $p = 0.013$; Figures 5A–5C). This further indicates that the POA projection of DMH galaninergic neurons is REM suppressing.

We next tested the effect of inactivating the POA-projecting DMH galaninergic neurons. To express the inhibitory opsin iC++ in these neurons (Berndt et al., 2016), we injected Cre-inducible rAAV2-retro-EF1α-DIO-iC++-eYFP into the POA of GAL-Cre mice. Laser stimulation (constant light, 1 min/trial, randomly applied every 5–30 min) significantly increased REM sleep (mean 12.6%, 95% CIs [9.2%, 16.2%], $p < 0.001$) and decreased NREM sleep (mean –10.7%, 95% CIs [−6.5%, –15.1%], $p < 0.05$; Figures 6A–6C). Furthermore, while the probability of a REM sleep episode initiated shortly (<120 s) after the end of the preceding REM episode was quite low before laser onset (2.4%), the probability increased to 18.1% for the REM episodes initiated during inactivation of the POA-projecting galaninergic neurons. In control mice expressing eGFP without ChR2 or iC++, laser stimulation had no effect ($p > 0.7$; Figures S6A–S6C), and the effects of laser stimulation were significantly

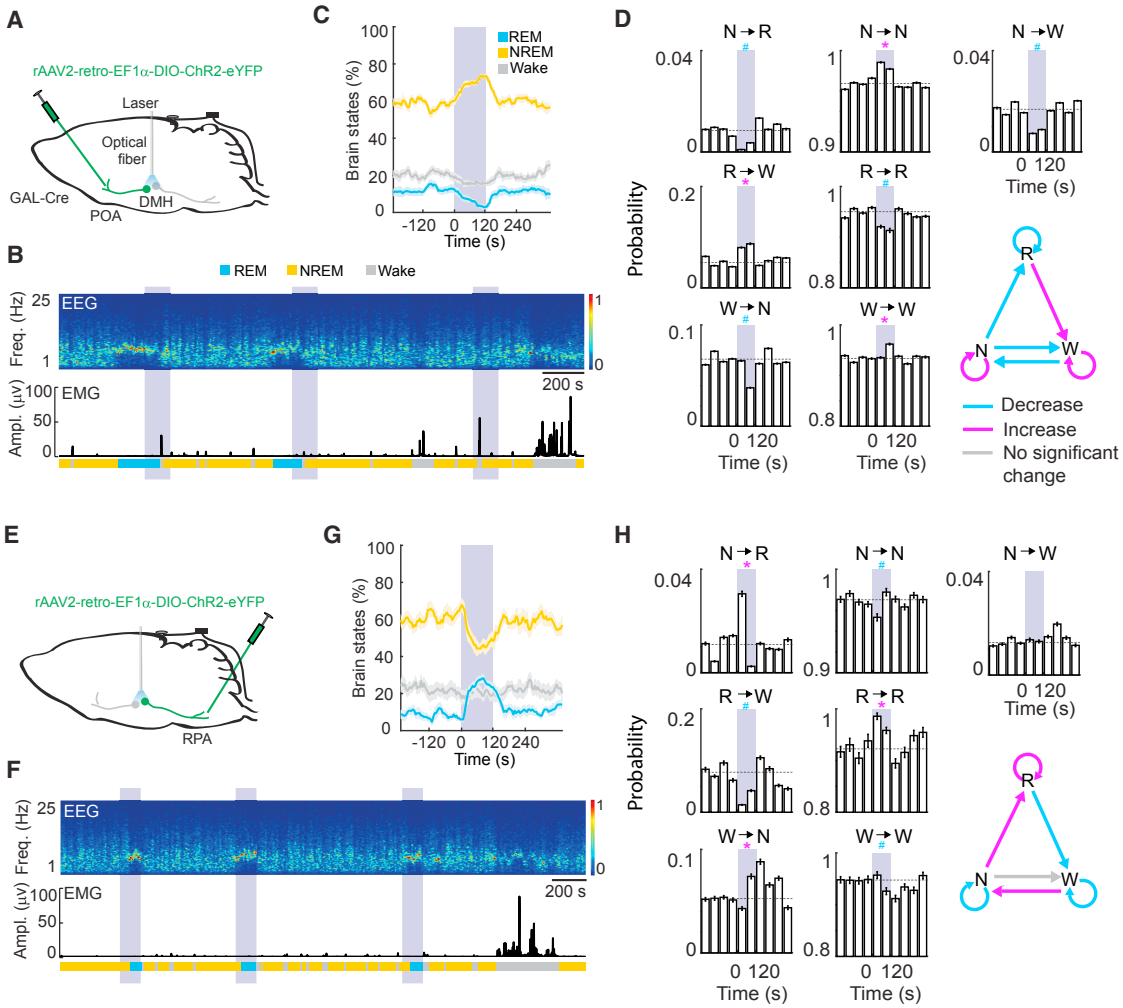

Figure 4. POA- and RPA-Projecting DMH Galaninergic Neurons Have Opposing Effects on REM-NREM Sleep Regulation

(A) Schematic of optogenetic activation of POA-projecting DMH galaninergic neurons.

(B) An example experiment showing EEG power spectrogram, EMG trace, and brain states (color coded). Purple shading, laser stimulation period.

(C) Percentage of time in NREM, REM, or wake state before, during, and after laser stimulation (purple shading), averaged from 6 mice. Shading of each trace, ±SEM.

(D) Transition probability within each 10 s period with optogenetic activation of POA-projecting DMH galaninergic neurons (n = 6 mice). Shown in each bar is the transition probability averaged across six consecutive 10 s bins within each 60 s. Error bar, 95% confidence interval (bootstrap). The baseline transition probability (gray dashed line) was averaged across all time bins within 240 s before laser onset. Direct wake→REM and REM→NREM transitions were not observed and the corresponding plots were omitted. Bottom right diagram indicates transition probabilities that are significantly increased, decreased, or unaffected by laser stimulation.

(E–H) Similar to (A)–(D), for optogenetic activation of RPA-projecting neurons (n = 4 mice). The percentage of NREM→REM transitions was 22.7% during laser and 9.9% during the 2-min period immediately before laser. The probability of REM episodes initiated <120 s following the preceding episode was 4.1% before laser and 19.2% during laser.

See also Figures S4–S6.

different between ChR2 and eGFP mice ($p < 0.001$, bootstrap) and between iC++ and eGFP mice ($p < 0.001$).

RPA-Projecting Neurons Promote REM and Suppress NREM Sleep

Finally, we tested the effects of activating and inactivating the RPA-projecting DMH galaninergic neurons. After injecting Cre-inducible rAAV2-retro-ChR2-eYFP into the RPA of GAL-Cre mice, laser stimulation in the DMH strongly increased REM sleep (mean 15.4%, 95% CIs [9.1%, 21.8%]; $p < 0.001$, bootstrap) and decreased NREM sleep (mean −13.9%, 95% CIs [−6.9%, −21.0%], $p < 0.001$; Figures 4E–4G and S5B). These effects were caused by increases in both NREM→REM and REM→REM transitions (Figure 4H), indicating enhancement of both the initiation and maintenance of REM sleep. In contrast, iC++-mediated inactivation of these neurons caused decreased REM sleep (mean −4.7%, 95% CIs [−2.3%, −7.3%], $p = 0.014$) and increased NREM sleep (mean 3.6%, 95% CIs [0.3%, 6.7%], $p = 0.029$;

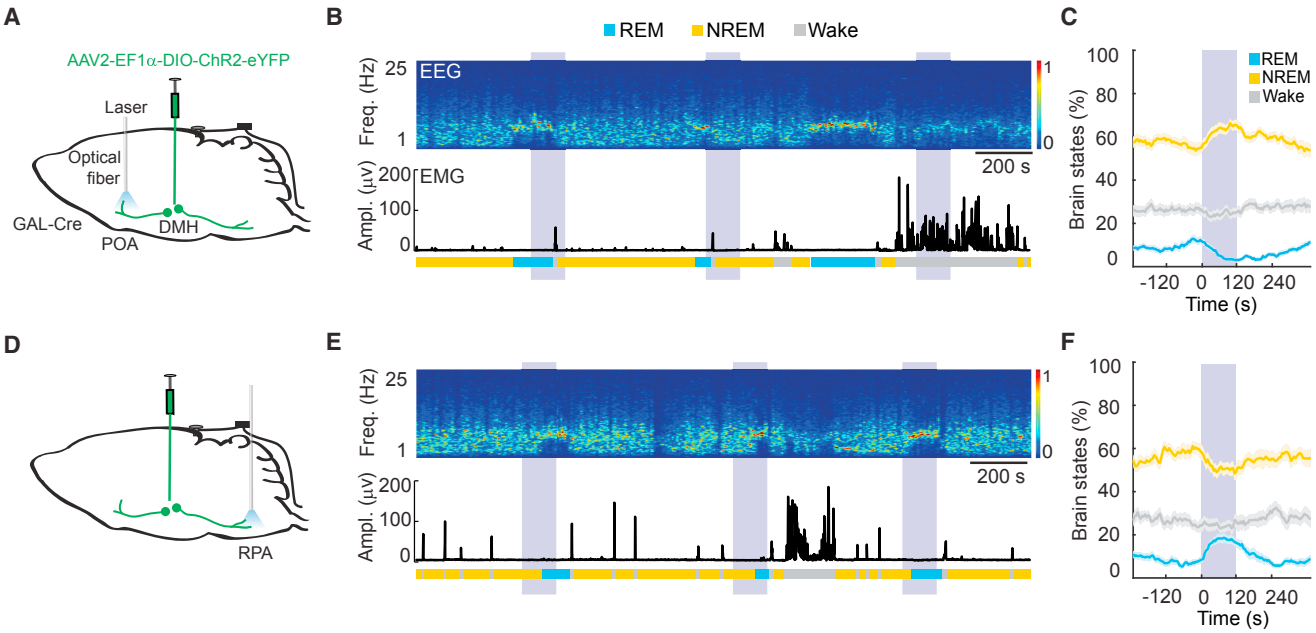

Figure 5. Optogenetic Activation of Axon Projections of DMH Galaninergic Neurons into the POA and RPA

(A) Schematic of optogenetic activation of DMH galaninergic axons in the POA.

(B) An example experiment showing EEG power spectrogram, EMG trace, and brain states (color coded). Purple shading, laser stimulation period.

(C) Percentage of time in NREM, REM, or wake state before, during, and after laser stimulation (purple shading) of DMH axons in the POA (n = 6 mice). Shading of each trace, ±SEM.

(D–F) Similar to (A)–(C), for optogenetic activation of DMH axons in the RPA (n = 4 mice).

Figures 6D–6F). Laser had no effect in control mice expressing eGFP alone ($p > 0.5$; Figures S6D–S6F), and the effects of laser stimulation were significantly different between ChR2 and eGFP mice ($p < 0.001$; bootstrap) and between iC++ and eGFP mice ($p = 0.038$). Furthermore, in GAL-Cre mice injected with AAV2-EF1α-DIO-ChR2-eYFP in their DMH, laser stimulation of the axons in the RPA increased REM sleep (mean 9.5%, 95% CIs [5.9%, 13.0%]; $p < 0.001$, bootstrap) and suppressed NREM sleep (mean –7.6%, 95% CIs [−3.3%, −11.9%], $p = 0.011$; Figures 5D–5F). Together, these results indicate that the RPA-projecting DMH galaninergic neurons are REM promoting.

DISCUSSION

Using cell-type- and projection-target-specific imaging and optogenetic manipulations, we have revealed a novel hypothalamic mechanism regulating the REM-NREM switch. While the DMH GABAergic neurons exhibit highly diverse brain-state-dependent calcium activity (Figure 1D, gray dots), the neuropeptide galanin labels two distinct subpopulations that are either REM-on or REM-off (Figures 1D, black dots). Retrograde labeling based on their axon projections then allowed us to isolate each of the two subsets and demonstrate their opposing effects on REM versus NREM sleep.

Earlier transection studies by Jouvet showed that the main brain region controlling REM sleep lies in the brainstem (Jouvet, 1962). The DMH galaninergic neurons characterized in our study are likely to interact with the brainstem REM circuit. The REM-promoting effect of RPA-projecting neurons could be partly mediated by their GABAergic and/or galaninergic inhibition of the serotonergic neurons in the RPA, which are known to be REM-off (Heym et al., 1982; Trulson and Trulson, 1982). These serotonergic neurons may in turn interact with other neurons in the REM-sleep control circuit (Moazzami et al., 2010), including GABAergic neurons in the ventral medulla (Weber et al., 2015). The POA-projecting neurons, on the other hand, could suppress REM sleep through multiple projections (Figures S2C, S2D, and S2G). In addition to the REM-promoting neurons in the POA (Chung et al., 2017; Lu et al., 2006), the REM-active, REM-promoting MCH neurons (Blanco-Centurion et al., 2016; Ferreira et al., 2017; Hassani et al., 2009; Jego et al., 2013) are located well within the axonal field of the POA-projecting neurons. Whether and how the DMH galaninergic neurons interact with these sleep-related neurons remain to be elucidated. Interestingly, the DMH, POA, and RPA are all key brain structures involved in thermoregulation (Morrison and Nakamura, 2011), an important homeostatic process closely related to sleep generation. In future studies it would be of great interest to investigate the relationship between the neurons controlling sleep and those regulating body temperature.

The nature of the inputs that give rise to the REM-on versus REM-off activity of the DMH galaninergic neurons remains unknown. A promising approach is to map the monosynaptic inputs to POA- or RPA-projecting galaninergic neurons using the "cell-type-specific tracing the relationship between input and output" (cTRIO) method (Beier et al., 2015; Schwarz et al.,

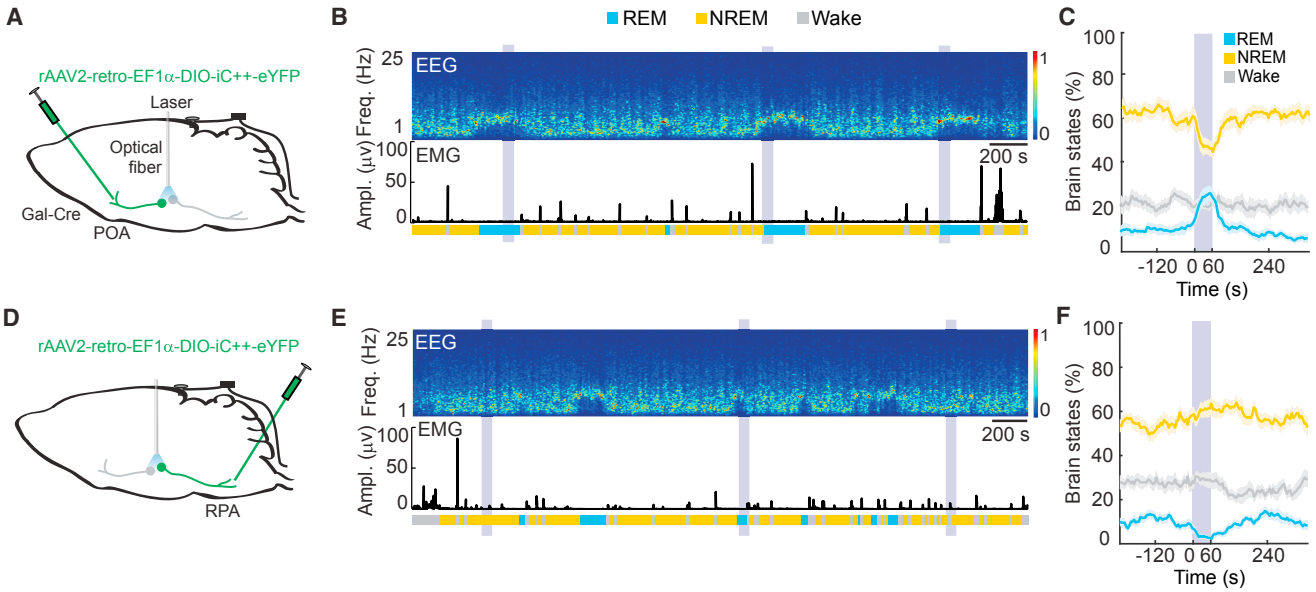

Figure 6. Effects of Optogenetic Inactivation of POA- and RPA-Projecting DMH Galaninergic Neurons

(A) Schematic of optogenetic inhibition of POA-projecting DMH galaninergic neurons.

(B) An example experiment showing EEG power spectrogram, EMG trace, and brain states (color coded). Purple shading, laser stimulation period.

(C) Percentage of time in NREM, REM, or wake state before, during, and after laser stimulation (purple shading), averaged from 6 mice. Shading of each trace, ±SEM. The percentage of NREM→REM transitions was 10.8% during laser and 5.8% during the 1-min period immediately before laser.

(D–F) Similar to (A)–(C), for optogenetic inhibition of RPA-projecting neurons (n = 4 mice). The percentage of NREM→REM transitions was 1.5% during laser and 5.4% during the 1-min period immediately before laser.

See also Figure S6.

2015). Such whole-brain mapping will provide an anatomical blueprint to guide functional identification of the REM- and NREM-sleep-related inputs. Another useful approach is to combine retrograde labeling and gene expression profiling to identify molecular markers specific for the POA- and RPA-projecting populations (Chung et al., 2017). Uncovering the genetic identity of each population will greatly facilitate selective targeting of these neurons for further circuit analysis.

Our results demonstrate a striking circuit motif in which two groups of neurons, residing in the same nucleus and using the same neurotransmitters (both GABA and galanin), promote two mutually exclusive brain states. The spatial intermingling between these two groups raises the intriguing possibility of local reciprocal inhibition, and their physical proximity could greatly improve the efficiency of the neuronal circuit in regulating the switch between REM and NREM sleep.

STAR★METHODS

Detailed methods are provided in the online version of this paper and include the following:

SUPPLEMENTAL INFORMATION

Supplemental Information includes six figures and can be found with this article online at https://doi.org/10.1016/j.neuron.2018.02.005.

ACKNOWLEDGMENTS

We thank F. Weber and P. Zhong for discussions and N. Wakamoto, A. Tran, M. Chang, and X. Chen for technical support. GCaMP6f was provided by V. Jayaraman, R.A. Kerr, D.S. Kim, L.L. Looger, and K. Svoboda from the GENIE Project. This work was supported by funding from Howard Hughes Medical Institute.

AUTHOR CONTRIBUTIONS

K.-S.C. and Y.D. designed experiments and wrote the manuscript. K.-S.C. and M.X. conducted the experiments. K.-S.C., M.X., and Y.D. analyzed data. Z.Z. prepared the AAV-retro virus. W.-C.C. prepared the virus for rabies virus experiments. T.G. and D.V.S. generated the AAV-retro plasmid. Y.D. supervised the project.

DECLARATION OF INTERESTS

D.V.S. is an inventor on patents and co-founder of a company related to AAV engineering.

Received: August 22, 2017
Revised: December 3, 2017
Accepted: February 2, 2018
Published: February 22, 2018

REFERENCES

Anaclet, C., Ferrari, L., Arrigoni, E., Bass, C.E., Saper, C.B., Lu, J., and Fuller, P.M. (2014). The GABAergic parafacial zone is a medullary slow wave sleep-promoting center. Nat. Neurosci. *17*, 1217–1224.

Aserinsky, E., and Kleitman, N. (1953). Regularly occurring periods of eye motility, and concomitant phenomena, during sleep. Science *118*, 273–274.

Aston-Jones, G., Chen, S., Zhu, Y., and Oshinsky, M.L. (2001). A neural circuit for circadian regulation of arousal. Nat. Neurosci. *4*, 732–738.

Beier, K.T., Steinberg, E.E., DeLoach, K.E., Xie, S., Miyamichi, K., Schwarz, L., Gao, X.J., Kremer, E.J., Malenka, R.C., and Luo, L. (2015). Circuit architecture of VTA dopamine neurons revealed by systematic input-output mapping. Cell *162*, 622–634.

Berndt, A., Lee, S.Y., Wietek, J., Ramakrishnan, C., Steinberg, E.E., Rashid, A.J., Kim, H., Park, S., Santoro, A., Frankland, P.W., et al. (2016). Structural foundations of optogenetics: Determinants of channelrhodopsin ion selectivity. Proc. Natl. Acad. Sci. USA *113*, 822–829.

Blanco-Centurion, C., Liu, M., Konadhode, R.P., Zhang, X., Pelluru, D., van den Pol, A.N., and Shiromani, P.J. (2016). Optogenetic activation of melanin-concentrating hormone neurons increases non-rapid eye movement and rapid eye movement sleep during the night in rats. Eur. J. Neurosci. *44*, 2846–2857.

Boissard, R., Fort, P., Gervasoni, D., Barbagli, B., and Luppi, P.H. (2003). Localization of the GABAergic and non-GABAergic neurons projecting to the sublaterodorsal nucleus and potentially gating paradoxical sleep onset. Eur. J. Neurosci. *18*, 1627–1639.

Brown, R.E., Basheer, R., McKenna, J.T., Strecker, R.E., and McCarley, R.W. (2012). Control of sleep and wakefulness. Physiol. Rev. *92*, 1087–1187.

Chen, T.-W., Wardill, T.J., Sun, Y., Pulver, S.R., Renninger, S.L., Baohan, A., Schreiter, E.R., Kerr, R.A., Orger, M.B., Jayaraman, V., et al. (2013). Ultrasensitive fluorescent proteins for imaging neuronal activity. Nature *499*, 295–300.

Chou, T.C., Scammell, T.E., Gooley, J.J., Gaus, S.E., Saper, C.B., and Lu, J. (2003). Critical role of dorsomedial hypothalamic nucleus in a wide range of behavioral circadian rhythms. J. Neurosci. *23*, 10691–10702.

Chung, S., Weber, F., Zhong, P., Tan, C.L., Nguyen, T.N., Beier, K.T., Hörmann, N., Chang, W.-C., Zhang, Z., Do, J.P., et al. (2017). Identification of preoptic sleep neurons using retrograde labelling and gene profiling. Nature *545*, 477–481.

Clément, O., Sapin, E., Bérod, A., Fort, P., and Luppi, P.H. (2011). Evidence that neurons of the sublaterodorsal tegmental nucleus triggering paradoxical (REM) sleep are glutamatergic. Sleep (Basel) *34*, 419–423.

Cox, J., Pinto, L., and Dan, Y. (2016). Calcium imaging of sleep-wake related neuronal activity in the dorsal pons. Nat. Commun. *7*, 10763.

Dement, W. (1958). The occurrence of low voltage, fast, electroencephalogram patterns during behavioral sleep in the cat. Electroencephalogr. Clin. Neurophysiol. *10*, 291–296.

Do, J.P., Xu, M., Lee, S.H., Chang, W.C., Zhang, S., Chung, S., Yung, T.J., Fan, J.L., Miyamichi, K., Luo, L., et al. (2016). Cell type-specific long-range connections of basal forebrain circuit. eLife *5*, 5.

Ferreira, J.G.P., Bittencourt, J.C., and Adamantidis, A. (2017). Melanin-concentrating hormone and sleep. Curr. Opin. Neurobiol. *44*, 152–158.

Findlay, A.L., and Hayward, J.N. (1969). Spontaneous activity of single neurones in the hypothalamus of rabbits during sleep and waking. J. Physiol. *201*, 237–258.

Gerfen, C.R., Paletzki, R., and Heintz, N. (2013). GENSAT BAC cre-recombinase driver lines to study the functional organization of cerebral cortical and basal ganglia circuits. Neuron *80*, 1368–1383.

Ghosh, K.K., Burns, L.D., Cocker, E.D., Nimmerjahn, A., Ziv, Y., Gamal, A.E., and Schnitzer, M.J. (2011). Miniaturized integration of a fluorescence microscope. Nat. Methods *8*, 871–878.

Hassani, O.K., Lee, M.G., and Jones, B.E. (2009). Melanin-concentrating hormone neurons discharge in a reciprocal manner to orexin neurons across the sleep-wake cycle. Proc. Natl. Acad. Sci. USA *106*, 2418–2422.

Hayashi, Y., Kashiwagi, M., Yasuda, K., Ando, R., Kanuka, M., Sakai, K., and Itohara, S. (2015). Cells of a common developmental origin regulate REM/non-REM sleep and wakefulness in mice. Science *350*, 957–961.

Heym, J., Steinfels, G.F., and Jacobs, B.L. (1982). Activity of serotonin-containing neurons in the nucleus raphe pallidus of freely moving cats. Brain Res. *251*, 259–276.

Hobson, J.A., McCarley, R.W., and Wyzinski, P.W. (1975). Sleep cycle oscillation: reciprocal discharge by two brainstem neuronal groups. Science *189*, 55–58.

Jego, S., Glasgow, S.D., Herrera, C.G., Ekstrand, M., Reed, S.J., Boyce, R., Friedman, J., Burdakov, D., and Adamantidis, A.R. (2013). Optogenetic identification of a rapid eye movement sleep modulatory circuit in the hypothalamus. Nat. Neurosci. *16*, 1637–1643.

Jouvet, M. (1962). [Research on the neural structures and responsible mechanisms in different phases of physiological sleep]. Arch. Ital. Biol. *100*, 125–206.

Konadhode, R.R., Pelluru, D., Blanco-Centurion, C., Zayachkivsky, A., Liu, M., Uhde, T., Glen, W.B., Jr., van den Pol, A.N., Mulholland, P.J., and Shiromani, P.J. (2013). Optogenetic stimulation of MCH neurons increases sleep. J. Neurosci. *33*, 10257–10263.

Lu, J., Sherman, D., Devor, M., and Saper, C.B. (2006). A putative flip-flop switch for control of REM sleep. Nature *441*, 589–594.

Maheshri, N., Koerber, J.T., Kaspar, B.K., and Schaffer, D.V. (2006). Directed evolution of adeno-associated virus yields enhanced gene delivery vectors. Nat. Biotechnol. *24*, 198–204.

Miyamichi, K., Amat, F., Moussavi, F., Wang, C., Wickersham, I., Wall, N.R., Taniguchi, H., Tasic, B., Huang, Z.J., He, Z., et al. (2011). Cortical representations of olfactory input by trans-synaptic tracing. Nature *472*, 191–196.

Moazzami, A., Tjen-A-Looi, S.C., Guo, Z.-L., and Longhurst, J.C. (2010). Serotonergic projection from nucleus raphe pallidus to rostral ventrolateral medulla modulates cardiovascular reflex responses during acupuncture. J. Appl. Physiol. *108*, 1336–1346.

Morrison, S.F., and Nakamura, K. (2011). Central neural pathways for thermoregulation. Front. Biosci. *16*, 74–104.

Mukamel, E.A., Nimmerjahn, A., and Schnitzer, M.J. (2009). Automated analysis of cellular signals from large-scale calcium imaging data. Neuron *63*, 747–760.

Oh, S.W., Harris, J.A., Ng, L., Winslow, B., Cain, N., Mihalas, S., Wang, Q., Lau, C., Kuan, L., Henry, A.M., et al. (2014). A mesoscale connectome of the mouse brain. Nature *508*, 207–214.

Osakada, F., and Callaway, E.M. (2013). Design and generation of recombinant rabies virus vectors. Nat. Protoc. *8*, 1583–1601.

Pinto, L., and Dan, Y. (2015). Cell-type-specific activity in prefrontal cortex during goal-directed behavior. Neuron *87*, 437–450.

Resendez, S.L., Jennings, J.H., Ung, R.L., Namboodiri, V.M.K., Zhou, Z.C., Otis, J.M., Nomura, H., McHenry, J.A., Kosyk, O., and Stuber, G.D. (2016). Visualization of cortical, subcortical and deep brain neural circuit dynamics during naturalistic mammalian behavior with head-mounted microscopes and chronically implanted lenses. Nat. Protoc. *11*, 566–597.

Romanov, R.A., Zeisel, A., Bakker, J., Girach, F., Hellysaz, A., Tomer, R., Alpár, A., Mulder, J., Clotman, F., Keimpema, E., et al. (2017). Molecular interrogation of hypothalamic organization reveals distinct dopamine neuronal subtypes. Nat. Neurosci. *20*, 176–188.

Saper, C.B., Fuller, P.M., Pedersen, N.P., Lu, J., and Scammell, T.E. (2010). Sleep state switching. Neuron *68*, 1023–1042.

Sapin, E., Lapray, D., Bérod, A., Goutagny, R., Léger, L., Ravassard, P., Clément, O., Hanriot, L., Fort, P., and Luppi, P.H. (2009). Localization of the brainstem GABAergic neurons controlling paradoxical (REM) sleep. PLoS ONE *4*, e4272.

Sastre, J.P., Buda, C., Kitahama, K., and Jouvet, M. (1996). Importance of the ventrolateral region of the periaqueductal gray and adjacent tegmentum in the control of paradoxical sleep as studied by muscimol microinjections in the cat. Neuroscience *74*, 415–426.

Scammell, T.E., Arrigoni, E., and Lipton, J.O. (2017). Neural circuitry of wakefulness and sleep. Neuron *93*, 747–765.

Schwarz, L.A., Miyamichi, K., Gao, X.J., Beier, K.T., Weissbourd, B., DeLoach, K.E., Ren, J., Ibanes, S., Malenka, R.C., Kremer, E.J., and Luo, L. (2015). Viral-genetic tracing of the input-output organization of a central noradrenaline circuit. Nature *524*, 88–92.

Sherin, J.E., Elmquist, J.K., Torrealba, F., and Saper, C.B. (1998). Innervation of histaminergic tuberomammillary neurons by GABAergic and galaninergic neurons in the ventrolateral preoptic nucleus of the rat. J. Neurosci. *18*, 4705–4721.

Steiger, A., and Holsboer, F. (1997). Neuropeptides and human sleep. Sleep *20*, 1038–1052.

Tervo, D.G., Hwang, B.Y., Viswanathan, S., Gaj, T., Lavzin, M., Ritola, K.D., Lindo, S., Michael, S., Kuleshova, E., Ojala, D., et al. (2016). A designer AAV variant permits efficient retrograde access to projection neurons. Neuron *92*, 372–382.

Trulson, M.E., and Trulson, V.M. (1982). Activity of nucleus raphe pallidus neurons across the sleep-waking cycle in freely moving cats. Brain Res. *237*, 232–237.

Tsunematsu, T., Ueno, T., Tabuchi, S., Inutsuka, A., Tanaka, K.F., Hasuwa, H., Kilduff, T.S., Terao, A., and Yamanaka, A. (2014). Optogenetic manipulation of activity and temporally controlled cell-specific ablation reveal a role for MCH neurons in sleep/wake regulation. J. Neurosci. *34*, 6896–6909.

Van Dort, C.J., Zachs, D.P., Kenny, J.D., Zheng, S., Goldblum, R.R., Gelwan, N.A., Ramos, D.M., Nolan, M.A., Wang, K., Weng, F.J., et al. (2015). Optogenetic activation of cholinergic neurons in the PPT or LDT induces REM sleep. Proc. Natl. Acad. Sci. USA *112*, 584–589.

Weber, F., and Dan, Y. (2016). Circuit-based interrogation of sleep control. Nature *538*, 51–59.

Weber, F., Chung, S., Beier, K.T., Xu, M., Luo, L., and Dan, Y. (2015). Control of REM sleep by ventral medulla GABAergic neurons. Nature *526*, 435–438.

Xu, M., Chung, S., Zhang, S., Zhong, P., Ma, C., Chang, W.C., Weissbourd, B., Sakai, N., Luo, L., Nishino, S., and Dan, Y. (2015). Basal forebrain circuit for sleep-wake control. Nat. Neurosci. *18*, 1641–1647.

Zhang, S., Xu, M., Chang, W.-C., Ma, C., Hoang Do, J.P., Jeong, D., Lei, T., Fan, J.L., and Dan, Y. (2016). Organization of long-range inputs and outputs of frontal cortex for top-down control. Nat. Neurosci. *19*, 1733–1742.

STAR★METHODS

KEY RESOURCES TABLE

REAGENT or RESOURCE	SOURCE	IDENTIFIER
Antibodies		
Green Fluorescent Protein (GFP) Antibody	Aves Labs	GFP-1020; RRID: AB_10000240
Bacterial and Virus Strains		
AAV2-EF1α-DIO-ChR2–eYFP	University of North Carolina Vector Core	N/A
AAV2-EF1α-DIO–eYFP	University of North Carolina Vector Core	N/A
AAV1-Syn-DIO-GCaMP6f	University of Pennsylvania Vector Core	AV-1-PV2819
rAAV2-retro-EF1α-DIO-ChR2-eYFP	This paper	Tervo et al., 2016
rAAV2-retro-EF1α-DIO-iC++-eYFP	This paper	Tervo et al., 2016
rAAV2-retro-EF1α-DIO-GCaMP6s	This paper	Tervo et al., 2016
rAAV2-retro-EF1α-DIO-mCherry	This paper	Tervo et al., 2016
rAAV2-retro-EF1α-DIO-eGFP	This paper	Tervo et al., 2016
RV-ΔG-eGFP+EnvA	This paper	Miyamichi et al., 2011
AAV2-EF1α-DIO-TVA-tdTomato	This paper	Miyamichi et al., 2011
Experimental Models: Organisms/Strains		
GAL-Cre mice	GENSAT	KI87; RRID: MMRRC_031060-UCD
GAD2-Cre mice	Jackson Laboratory	010802; RRID: IMSR_JAX:010802
Software and Algorithms		
MATLAB	MathWorks	R2016b
nVista HD software	Inscopix	N/A
Mosaic	Inscopix	1.2
OpenEx software	TDT	N/A
ImageJ	NIH	https://imagej.nih.gov/ij/
Other		
nVista system	Inscopix	Version 1
GRIN lens	Inscopix	1050-002179
TDT system	TDT	3
TDT amplifier	TDT	RZ5
Nanozoomer	Hamamatsu	N/A

CONTACT FOR REAGENT AND RESOURCE SHARING

Further information and requests for resources and reagents should be directed to and will be fulfilled by the Lead Contact, Yang Dan (ydan@berkeley.edu).

EXPERIMENTAL MODEL AND SUBJECT DETAILS

All experimental procedures were approved by the Animal Care and Use Committee at the University of California, Berkeley. Optogenetic manipulation and viral tracing experiments were performed in male or female GAL-Cre mice (GENSAT, stock number KI87). Calcium imaging experiments were performed in male or female GAL-Cre mice and GAD2-Cre mice (Jackson Laboratory, stock numbers 010802). Animals were housed on a 12-hr dark/12-hr light cycle (light on between 7:00 and 19:00). Animals with implants for EEG/EMG recordings, optogenetic stimulation or calcium imaging were housed individually. Adult (6- to 12-week old) mice were used for surgery.

For optogenetic experiments, GAL-Cre mice were randomly assigned to control (injected with AAV expressing eGFP) and experimental groups (injected with AAV expressing ChR2-eYFP or iC++-eYFP). For optogenetic, imaging, and rabies-mediated tracing experiments, GAL-Cre mice were randomly assigned to POA- or RPA- retrograde experiments. No randomization was used for

calcium imaging (for both GAL-Cre and GAD2-Cre mice) and AAV anterograde tracing (GAL-Cre mice). Investigators were not blinded to animal identity and outcome assessment.

METHOD DETAILS

Surgical Procedures

Adult mice were anaesthetized with isoflurane (5% induction, 1.5% maintenance) and placed on a stereotaxic frame. Body temperature was kept stable throughout the procedure with a heating pad. After asepsis, the skin was incised to expose the skull, and the overlying connective tissue was removed. A craniotomy (0.5-1 mm diameter) was made for virus injection, optical fiber implantation, or GRIN lens implantation. The stereotaxic coordinates were as follows. DMH: anteroposterior (AP) –1.5 mm, mediolateral (ML) 0.3 mm, dorsoventral (DV) 4.8-5.0 mm; POA: AP 0 mm, ML 0.3 mm, DV 5.0-5.2 mm; RPA: AP –6 mm, ML 0 mm, DV 5.6-5.8 mm.

The following viral vectors were used in this study. AAV2-EF1α-DIO-ChR2–eYFP, AAV2-EF1α-DIO–eYFP (produced by University of North Carolina Vector Core), AAV1-Syn-DIO-GCaMP6f (University of Pennsylvania Vector Core, $\sim 10^{12}$ vector genomes per milliliter; injection after 10 × dilution), rAAV2-retro-EF1α-DIO-ChR2-eYFP, rAAV2-retro-EF1α-DIO-iC++-eYFP, rAAV2-retro-EF1α-DIO-GCaMP6s, rAAV2-retro-EF1α-DIO-mCherry, rAAV2-retro-EF1α-DIO-eGFP, AAV2-CAG-DIO-TVA-mCherry (10^{12} to 10^{13} vector genomes per milliliter; AAV preparation followed previously reported protocol (Maheshri et al., 2006; Zhang et al., 2016)) and RV-ΔG-eGFP+EnvA (10^8 to 10^9 vector genomes per milliliter; preparation followed previously reported protocol (Osakada and Callaway, 2013; Zhang et al., 2016)). For injection, virus was loaded into a sharp micropipette mounted on a Nanoject II attached to a micromanipulator and slowly injected into the target area (for imaging, 500 nL unilateral, into DMH, POA or RPA; for optogenetic activation of DMH galaninergic neurons or their axons, 500 nL/hemisphere, bilateral, into the DMH; for optogenetic manipulation of POA-projecting neurons, 500 nL/hemisphere, bilateral, into the POA; for optogenetic manipulations of RPA-projecting neurons, 600 nL into the RPA). To trace the axon collaterals of subgroups of DMH galaninergic neurons projecting to either the POA or the RPA, AAV2-CAG-DIO-TVA-mCherry was first injected into the DMH (500 nL, unilateral) of GAL-Cre mice. Three weeks later, RV-ΔG-eGFP+EnvA (500 nL) was injected into the POA or RPA of these mice.

For EEG and EMG recordings, a reference screw was inserted into the skull on top of the cerebellum. Two stainless steel screws were inserted into the skull 1.5 mm from midline and 1.5 mm anterior to the bregma, and two others were inserted 3 mm from the midline and 3.5 mm posterior to the bregma. One EMG electrode was inserted into the neck musculature. Insulated leads from the EEG and EMG electrodes were soldered to a pin header, which was secured to the skull using dental cement.

For calcium imaging, mice were implanted with a GRIN lens (600 μm diameter, 7.3 mm long, Inscopix). A 600 μm diameter optical fiber (Thorlabs) with sharpened tip was inserted into a polyimide tube (625 μm diameter, cut to 7.3 mm, Vention) and implanted to 200 μm above the target brain area. The polyimide tube was then secured to the skull using dental cement, and the optical fiber was retracted. The GRIN lens was then inserted through the polyimide tube into the target area. A heat-shrinkable tube with paper tape above was used as protective cap to cover the GRIN lens. After >3 weeks, the tape was removed to expose the GRIN lens and a miniaturized, single-photon, fluorescence microscope (Inscopix) was lowered over the implanted GRIN lens until the GCaMP6 fluorescence was visible under illumination with the microscope's LED. The microscope's baseplate was then secured to the skull with dental cement darkened with carbon powder for subsequent attachment of the microscope to the head. After recovery from surgery, we did not observe any gross behavioral abnormality, and these mice exhibited normal sleep–wake cycles. After surgery, mice were allowed to recover for at least 2 weeks before experiments.

For optogenetic manipulations, mice were implanted bilaterally with optical fibers. After surgery, mice were allowed to recover for at least 2 weeks before experiments.

Polysomnographic Recordings

EEG and EMG electrodes were connected to flexible recording cables via a mini-connector, and recordings were made in the animal's home cage placed in a sound-attenuated box. Recordings started after at least 1 hr of habituation after the experimenter connected the cables (which could disrupt the natural propensity for sleep). All signals were acquired using TDT RZ5 amplifier (bandpass filter, 1–750 Hz; sampling rate, 1,500 Hz). We used the difference between the voltage potentials recorded from the EEG electrode and the reference electrode as EEG signal and the difference between the potentials from the EMG electrode and reference electrode as EMG signal.

Optogenetic Manipulations

We performed optogenetic manipulation experiments 4 to 6 weeks after injection of AAV expressing ChR2. Recordings took place during the light cycle (10:00 to 19:00) in the mouse's home cage placed within a sound-attenuating chamber. For optogenetic manipulations of DMH neurons, each trial consists of a 20 Hz pulse train lasting for 120 s (for optogenetic activation) or constant light lasting for 60 s (for optogenetic inhibition) using a blue 473-nm laser (6 mW at fiber tip, Shanghai Laser). The inter-trial interval was randomly distributed, from 5 to 30 min, controlled by the TDT system.

Calcium Imaging

Imaging sessions took place during the light cycle in the home cage placed within a sound-attenuated chamber. The animal was briefly anesthetized with isoflurane to secure the microscope to the baseplate and to focus it to a given field of view. The animal was then allowed to recover from anesthesia and habituate in their home cage for at least 30 min prior to imaging. Calcium activity was acquired using the nVista hardware and nVista HD software (Inscopix), with a 5 Hz image acquisition rate using 0.2-0.7 mW illumination. EEG and EMG were acquired using TDT system-3 controlled by OpenEx software (TDT) (see above). An output signal (5 Hz) delivered from the Inscopix system to the TDT system throughout the recording session was used to synchronize the timing between the imaging and EEG/EMG recordings. Each recording session lasted 30-120 min, and for each mouse the data from a single recording session was included. Although GCaMP6f has faster calcium dynamics, the fluorescence signals are weaker than GCaMP6s. Since the expression efficiency of AAV-retro injected at the projection target is weaker than that of AAV1 injected in the DMH, we chose to use GCaMP6s for the imaging experiments involving retrograde labeling.

Histology and Immunohistochemistry

Mice were deeply anesthetized and transcardially perfused with 0.1M PBS followed by 4% paraformaldehyde in PBS. After removal, brains stayed overnight in 4% paraformaldehyde. For cryoprotection, brains were stored in 30% sucrose (w/v) in PBS solution for at least one night. Brains were sliced in 50 μm coronal sections using a cryostat (Thermo Scientific). For immunohistochemistry, non-specific binding sites were blocked by incubating the brain sections in 10% goat serum (Millipore) in PBST (0.3% Triton X-100 in PBS). To amplify the fluorescence of axon fibers expressing eYFP or eGFP we applied antibodies for GFP (GFP-1020, Aves Labs, 1:1,000). Brain sections were incubated with the primary antibody diluted in blocking solution for two nights. A species-specific secondary antibody conjugated with green Alexa fluorophore (1:1,000; goat anti chicken) was diluted in PBS and applied for 2 hr at room temperature. Fluorescence images were taken using 20 × , 0.75 NA objective in a high-throughput slide scanner Nanozoomer 2.0 RS (Hamamatsu), a fluorescence microscope (Olympus BX53) or a confocal microscope (LSM 710, Zeiss).

QUANTIFICATION AND STATISTICAL ANALYSIS

Polysomnographic Analysis

Spectral analysis was carried out using fast Fourier transform, and NREM, REM and wake states were semi-automatically classified using a custom-written sleep analysis software (MATLAB, MathWorks) for each 5 s epoch (wake: desynchronized EEG and high EMG activity; NREM sleep: synchronized EEG with high power at 0.5–4 Hz and low EMG activity; REM sleep: desynchronized EEG with high power at theta frequencies (6–9 Hz) and low EMG activity) (Xu et al., 2015). Brain state classification was validated by human after automatic scoring. For optogenetic experiments, we aligned all trials from the same experimental group of mice by the time of laser stimulation to quantify the effect.

Transition Analysis

To quantify transition probabilities between brain states, we discretized time into 10 s bins. The brain state of each bin was classified based on EEG and EMG recordings (see Polysomnographic Analysis above). We then aligned all laser stimulation trials from all N mice by the onset of laser stimulation at time 0. To determine the transition probability from state X to Y for time bin i, $P_i(X, Y)$, we first determined the number of trials (n) in which the animal was in brain state X during the preceding time bin i-1. Next, we identified the subset of these trials (m) in which the animal transitioned into state Y in the current time bin i. The transition probability $P_i(Y|X)$ was computed as m/n. In Figures 4D and 4H, each bar represents the transition probability averaged across six consecutive bins. To compute the baseline transition probabilities, we averaged across all time bins within 240 s before laser onset.

Calcium Imaging Analysis

Imaging data were processed in Mosaic (Inscopix) and MATLAB (MathWorks). First, the acquired images were spatially downsampled by a factor of 4. To correct for lateral motion of the brain relative to the GRIN lens, we used the motion correction function in Mosaic, as in previous studies (Mukamel et al., 2009; Resendez et al., 2016). Regions of interest (ROIs) were then identified using an established algorithm based on principal and independent component analyses (PCA-ICA) followed by visual inspection (Mukamel et al., 2009; Resendez et al., 2016). The pixel intensities within each ROI were averaged to create a fluorescence time-series. For individual neurons, the Z score was calculated as the difference between the calcium activity at each bin and the averaged calcium activity of the whole recording time, divided by the standard deviation of the whole recording time.

Activity map was computed as follows:

$$m_{x,y} = \left\langle \left\langle \left(f_{x,y}(t) - f_{x,y}\right) / \left(f_{x,y} + f\right) \right\rangle_w^3 \right\rangle_t$$

where $m_{x,y}$ is the activity at pixel (x,y), brackets indicate averaging, $f_{x,y}(t)$ is the fluorescence value at frame t, $f_{x,y}$ is the average of $f_{x,y}(t)$ over time, f is the average of $f_{x,y}$ over w, and w is a sliding window of 2 × 2 pixels (~5 × 5 μm)(Pinto and Dan, 2015).

Axon Arborization Analysis

Consecutive 50 μm coronal sections were collected and stained using Hoechst. Slides were scanned using a Nanozoomer (Hamamatsu). All images were acquired using identical settings and were analyzed using ImageJ and MATLAB as previously described (Chung et al., 2017). Images were background subtracted, thresholded, and pixels above this threshold were interpreted as positive signals. Pixels at the tissue borders with fluorescence artifact were excluded from the analysis. Each brain sample was aligned to the Allen Mouse Brain Atlas (Oh et al., 2014). The eGFP-labeled axon signal was quantified for each region and averaged across samples (Do et al., 2016; Zhang et al., 2016).

Statistics

Statistical analysis was performed using MATLAB. The selection of statistical tests was based on reported previous studies. All statistical tests were two-sided. The 95% confidence intervals for brain state probabilities were calculated using a bootstrap procedure: for an experimental group of n mice, with mouse i comprising mi trials, we repeatedly resampled the data by randomly drawing for each mouse mi trials (random sampling with replacement). For each of the 10,000 iterations, we recalculated the mean probabilities for each brain state across the n mice. The lower and upper confidence intervals were then extracted from the distribution of the resampled mean values. To test whether a given brain state was significantly modulated by laser stimulation, we calculated for each bootstrap iteration the difference between the mean probabilities during laser stimulation and the baseline values without laser stimulation (identical duration to laser stimulation). From the resulting distribution of difference values, we then calculated a p value to assess whether laser stimulation significantly modulated brain states or transitions between brain states. The investigators were not blinded to allocation during experiments and outcome assessment.